NASA/TM—2007-214966 AIAA–2007–3679

Numerical Technique for Analyzing Rotating Rake Mode Measurements in a Duct With Passive Treatment and Shear Flow

Milo D. Dahl and Daniel L. Sutliff
Glenn Research Center, Cleveland, Ohio

August 2007

NASA STI Program . . . in Profile

Since its founding, NASA has been dedicated to the advancement of aeronautics and space science. The NASA Scientific and Technical Information (STI) program plays a key part in helping NASA maintain this important role.

The NASA STI Program operates under the auspices of the Agency Chief Information Officer. It collects, organizes, provides for archiving, and disseminates NASA's STI. The NASA STI program provides access to the NASA Aeronautics and Space Database and its public interface, the NASA Technical Reports Server, thus providing one of the largest collections of aeronautical and space science STI in the world. Results are published in both non-NASA channels and by NASA in the NASA STI Report Series, which includes the following report types:

- TECHNICAL PUBLICATION. Reports of completed research or a major significant phase of research that present the results of NASA programs and include extensive data or theoretical analysis. Includes compilations of significant scientific and technical data and information deemed to be of continuing reference value. NASA counterpart of peer-reviewed formal professional papers but has less stringent limitations on manuscript length and extent of graphic presentations.

- TECHNICAL MEMORANDUM. Scientific and technical findings that are preliminary or of specialized interest, e.g., quick release reports, working papers, and bibliographies that contain minimal annotation. Does not contain extensive analysis.

- CONTRACTOR REPORT. Scientific and technical findings by NASA-sponsored contractors and grantees.

- CONFERENCE PUBLICATION. Collected papers from scientific and technical conferences, symposia, seminars, or other meetings sponsored or cosponsored by NASA.

- SPECIAL PUBLICATION. Scientific, technical, or historical information from NASA programs, projects, and missions, often concerned with subjects having substantial public interest.

- TECHNICAL TRANSLATION. English-language translations of foreign scientific and technical material pertinent to NASA's mission.

Specialized services also include creating custom thesauri, building customized databases, organizing and publishing research results.

For more information about the NASA STI program, see the following:

- Access the NASA STI program home page at *http://www.sti.nasa.gov*

- E-mail your question via the Internet to *help@sti.nasa.gov*

- Fax your question to the NASA STI Help Desk at 301–621–0134

- Telephone the NASA STI Help Desk at 301–621–0390

- Write to:
  NASA Center for AeroSpace Information (CASI)
  7115 Standard Drive
  Hanover, MD 21076–1320

NASA/TM—2007-214966 AIAA–2007–3679

Numerical Technique for Analyzing Rotating Rake Mode Measurements in a Duct With Passive Treatment and Shear Flow

Milo D. Dahl and Daniel L. Sutliff
Glenn Research Center, Cleveland, Ohio

Prepared for the
13th AIAA/CEAS Aeroacoustics Conference
sponsored by the American Institute of Aeronautics and Astronautics
Rome, Italy, May 21–23, 2007

National Aeronautics and
Space Administration

Glenn Research Center
Cleveland, Ohio 44135

August 2007

This report contains preliminary findings,
subject to revision as analysis proceeds.

This work was sponsored by the Fundamental Aeronautics Program
at the NASA Glenn Research Center.

Level of Review: This material has been technically reviewed by technical management.

Available from

NASA Center for Aerospace Information
7115 Standard Drive
Hanover, MD 21076–1320

National Technical Information Service
5285 Port Royal Road
Springfield, VA 22161

Available electronically at http://gltrs.grc.nasa.gov

Numerical Technique for Analyzing Rotating Rake Mode Measurements in a Duct With Passive Treatment and Shear Flow

Milo D. Dahl and Daniel L. Sutliff
National Aeronautics and Space Administration
Glenn Research Center
Cleveland, Ohio 44135

Abstract

A technique is presented for the analysis of measured data obtained from a rotating microphone rake system. The system is designed to measure the interaction modes of ducted fans. A Fourier analysis of the data from the rotating system results in a set of circumferential mode levels at each radial location of a microphone inside the duct. Radial basis functions are then least-squares fit to this data to obtain the radial mode amplitudes. For ducts with soft walls and mean flow, the radial basis functions must be numerically computed. The linear companion matrix method is used to obtain both the eigenvalues of interest, without an initial guess, and the radial basis functions. The governing equations allow for the mean flow to have a boundary layer at the wall. In addition, a nonlinear least-squares method is used to adjust the wall impedance to best fit the data in an attempt to use the rotating system as an in-duct wall impedance measurement tool. Simulated and measured data are used to show the effects of wall impedance and mean flow on the computed results.

I. Introduction

A diagnostic tool was needed to measure the interaction modes of ducted fans in order to develop fan tone noise reduction techniques. Cicon et al.[1] proposed a concept for a continuously rotating microphone rake that would be able to obtain all modal amplitudes in a reasonable data acquisition time. The key concept is that by slowly rotating the microphone rake in a manner locked to the fan shaft, a Doppler shift is imparted to the duct spinning modes that is uniquely based on the mode physics. The resulting rotating microphone rake system developed by the NASA Glenn Research Center (called the Rotating Rake Mode Measurement System or just the Rotating Rake) has made several advances in the understanding of turbofan mode generation.[2] Hall et al.[3] developed the original data analysis scheme for the Rotating Rake using closed form solutions that were readily obtained for hard wall, circular ducts with no mean flow. The Rotating Rake has been very successful in measuring the modal content propagating in hard wall ducts. The data analysis was extended by Sutliff[2] in an attempt to include the effects of a constant mean flow in a soft wall duct, whether circular or annular in cross-section. For a constant area duct, the basis functions were again obtained using closed form analytical solutions.

The initial processing of the data obtained from the Rotating Rake follows two basic steps: (1) The signals streaming from the microphones in the rake are digitized and a Fourier transform is applied. The Fourier coefficients represent the complex amplitudes of the circumferential modes of the measured acoustic pressure field in the duct. (2) Each circumferential mode is further decomposed into a series of radial basis or mode functions. This series of radial basis functions takes the form of a weighted sum of Bessel functions that are the closed formed solution to the governing wave equation in a circular or annular duct for the following conditions: (a) the walls of the duct are hard and there is no mean flow, (b) the walls of the duct are hard and there is a uniform mean flow, and (c) the walls of the duct are lined with a locally reacting impedance and there is no mean flow. For these cases, the orthogonal properties of the Bessel functions allow the complex amplitudes of the radial basis functions to be easily obtained from an integration of the

pressure disturbance across the area of the duct. These radial basis functions are linearly combined to fit the measured circumferential mode data in a least-squares sense. In addition, there is a closed form relation between the radial eigenvalue that is part of the argument of the Bessel function and the axial wave number, which determines the propagation and/or decay of the mode in the axial direction of the duct. The data analysis for constant mean flow in a soft wall duct proposed by Sutliff[2] simplified the analysis by applying the orthogonality principle to the radial basis functions in that case, even though the principle did not strictly apply.

For the general duct flow case where a boundary layer exists at the wall whether the wall is hard or soft, the previous data analysis using closed form solutions may not be sufficiently accurate. Example radial basis functions are shown in Figure 1 for hard wall and soft wall boundary conditions where the flow is varied from no flow to plug flow to using a flow profile. The no-flow and plug-flow cases have identical radial basis functions for the hard-wall boundary condition and small changes are seen in the radial basis functions for the soft wall case. For these soft-wall conditions, it is possible to use the no-flow radial basis functions for fitting rotating rake measured data in a soft wall duct within some error, hopefully small. When a mean flow profile is included when computing the radial basis functions (See Figure 9 for plots of the flow profile.), the results in Figure 1 show a definite change especially for the soft wall conditions. The $M_{Avg} = -0.25$ profile results represent approach conditions for a jet engine of the size typically used on business jets. The plot shows about a 1.4 dB peak mode amplitude change from the non-flow-profile case which would then effect the level of acoustic power contained in that mode. The desire to be accurate in determining the mode power in a soft wall duct with flow gives sufficient reason to further study the effects of shear flow on the data analysis where the governing equations do not have closed form solutions. A more general approach is proposed in this paper to the data analysis technique for the rotating rake system by developing a numerical approach to obtain the radial basis functions. The technique includes wall impedance boundary conditions and allows shear flow conditions to exist in the duct. In addition, the analysis provides for the possibility that the wall impedance is unknown in the least-square fit of the basis functions to the data. Since the impedance affects all the basis functions nonlinearly, the least-squares fit, in this case, is performed iteratively.

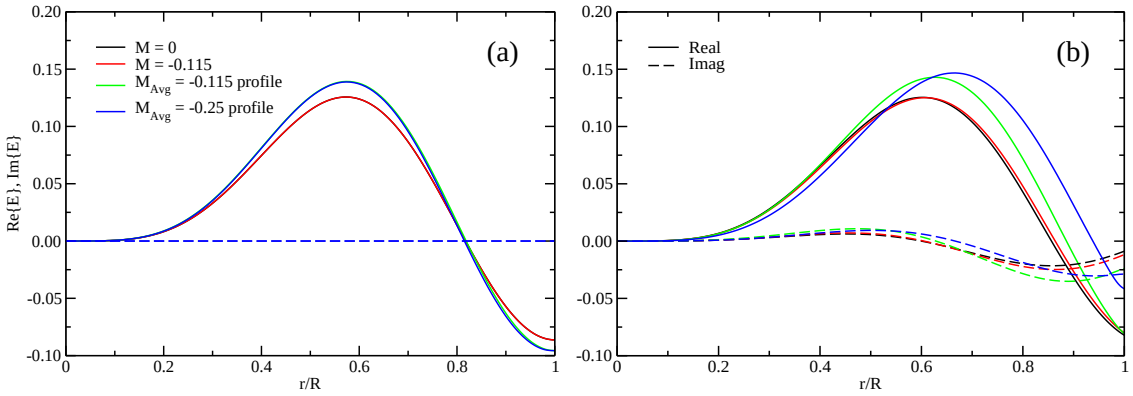

Figure 1. Comparison of radial basis functions computed using $m = 4$, $n = 1$, $\eta = 10.8$ with no flow, plug flow, and flow profile conditions. (a) Hard wall. (b) Soft wall with $Z = 1.7 - 2.2i$. Flow profiles used for calculations are shown in Figure 9.

In the next section, we present the governing equations for the propagation of sound in a cylindrical or annular duct while allowing for the presence of a general parallel mean flow. Using both hard and soft wall boundary conditions, an eigenvalue problem is formed that when solved produces both the complex axial wave numbers, the eigenvalues, and their associated radial basis functions, the eigen-functions. Since the eigenvalue appears nonlinearly in the governing equation, we use the linear companion matrix method to directly solve the eigenvalue problem. The method is globally convergent with no need for any initial guess eigenvalues unlike alternative approaches that use local iteration. Example results show the utility of the method. This is followed by a description of the least-squares procedures for solving for both the radial mode amplitudes and the wall impedance. The procedures are designed to accommodate the changing behavior of mode shapes and radial-mode order as the wall impedance changes. Finally, results are shown for fitting numerically generated radial basis functions to both simulated and measured data. For the latter, both plug flow and mean profile flow are used in the calculations.

II. Numerical Solution

The goal of analyzing the Rotating Rake data is to obtain the amplitude of the measured modes in the duct and, if desired, deduce the impedance of the installed duct wall acoustic treatment. Once the mode amplitudes are found, the acoustic power in each mode can be computed and compared to far field radiated power levels. For that to occur, two basic processes are followed: 1) determine the radial basis functions by numerically solving the eigenvalue problem presented by the governing equation and 2) determine the mode amplitudes by a least-squares fit and if the impedance is to be found, use an iteration approach.

II.A. Eigenvalue Problem

The numerical analysis of the eigenvalue problem is based on a discretization of the third order equation for the acoustic pressure p derived from combining the linearized momentum and energy equations, and assuming the static pressure is constant.

$$\frac{D^3p}{Dt^3} + c^2\left[2\,\frac{\partial(cM)}{\partial r}\,\frac{\partial^2 p}{\partial x\,\partial r} - \frac{1}{c^2}\,\frac{\partial c^2}{\partial r}\,\frac{D}{Dt}\,\frac{\partial p}{\partial r} - \frac{D}{Dt}\nabla^2 p\right] = 0 \tag{1}$$

where

$$\frac{D}{Dt} = \frac{\partial}{\partial t} + cM\,\frac{\partial}{\partial x}$$

and ∇^2 is the Laplace operator in cylindrical coordinates. This equation accounts for the compressibility of the flow and allows both the Mach number M and the speed of sound c to be functions of the radial direction. For subsonic flow in a duct, the conditions are such that the speed of sound is about constant. Hence, equation (1) reduces to that given by Eversman[4] (equation 13) in cylindrical coordinates.

For a circular or annular duct, the soft wall boundary condition for a locally reacting impedance is found by using the continuity of particle displacement. The general form of the boundary condition in terms of acoustic pressure at $r = R_o$, the outer wall, is

$$\frac{\partial^2 p}{\partial t\,\partial r} = -\overline{\rho}\hat{A}^*_{ow}\left[\frac{\partial}{\partial t} + cM\,\frac{\partial}{\partial x}\right]^2 p \tag{2}$$

where $\hat{A}^*_{ow}$ is the outer wall admittance and $\overline{\rho}$ is the mean flow density. (The wall impedance is related to the the wall admittance by $Z^* = 1/\hat{A}^*$.) This condition reduces to the pure admittance boundary condition when $M = 0$ at the wall for a boundary layer flow and reduces to the hard wall boundary condition when $\hat{A}^*_{ow} = 0$. For a circular duct, the boundary condition at the duct centerline, $r = 0$, is given by

$$\begin{aligned} \frac{\partial p}{\partial r} &= 0 \qquad m = 0 \\ p &= 0 \qquad m \neq 0 \end{aligned} \tag{3}$$

where m is the circumferential mode number. An annular duct may also have a soft wall boundary condition at the inner wall, $r = R_i$.

$$\frac{\partial^2 p}{\partial t\,\partial r} = \overline{\rho}\hat{A}^*_{iw}\left[\frac{\partial}{\partial t} + cM\,\frac{\partial}{\partial x}\right]^2 p \tag{4}$$

The sign difference between equations (2) and (4) follows from the convention that in the definition of the wall impedance, the particle velocity is defined as positive into the locally reacting impedance.

The analysis of equation (1) starts by using the separation of variables solution form for the acoustic pressure

$$p(x,\theta,r,t) = p_{mn}E_{mn}(r)e^{i(\omega t + m\theta - k_x x)} \tag{5}$$

where we let E_{mn} be a general function of r that forms the basis function for the least-squares fit, ω is the radian frequency, and k_x is the axial wave number which also depends on m and n. Equation (5) represents one term in a double summation over all circumferential mode numbers m and radial mode numbers n. Since equation (1) is linear, it can be solved using one mode at a time. Substitute into equation (1) and divide

out the exponential functions and the amplitude coefficient to obtain an equation that is used to determine the shape of the radial basis function E for each pair of (m, n) mode numbers.

$$\left[1 - cM\,\frac{k_x}{\omega}\right]^3 E + \frac{c^2}{\omega^2}\left(2\,\frac{k_x}{\omega}\frac{\partial(cM)}{\partial r}\frac{\partial E}{\partial r} + \frac{1}{c^2}\frac{\partial c^2}{\partial r}\left[1 - cM\,\frac{k_x}{\omega}\right]\frac{\partial E}{\partial r} + \left[1 - cM\,\frac{k_x}{\omega}\right]\left[\frac{\partial^2 E}{\partial r^2} + \frac{1}{r}\frac{\partial E}{\partial r} - \frac{m^2}{r^2}E - k_x^2 E\right]\right) = 0 \tag{6}$$

With boundary conditions defined by equations (2) to (4), the resulting equation becomes an eigenvalue problem where the eigenvalue is the complex axial wave number and the eigen-functions no longer have the form of Bessel functions that were found for the previous closed form solutions. Using finite difference approximations, equation (6) is discretized using $N + 1$ nodes resulting in a matrix equation that, including the appropriate boundary conditions, is written as

$$\mathbf{D}_3(k_x)\mathbf{E} = 0 \tag{7}$$

where $\mathbf{D}_3(k_x)$ is a lambda matrix of degree three representing a scalar polynomial with matrix coefficients

$$\mathbf{D}_3(k_x) = \mathbf{C}_0 k_x^3 + \mathbf{C}_1 k_x^2 + \mathbf{C}_2 k_x + \mathbf{C}_3 \tag{8}$$

and $\mathbf{E}$ is the vector of acoustic pressure basis function values at each node point.

The eigenvalues of equation (7) are easily found using the linear companion matrix method. Following Bridges & Morris,[5] we assemble the companion matrix. The $\mathbf{C}$ matrices in equation (8) are populated by values obtained from the discretization of equation (6) and its boundary conditions. The computational grid has uniform grid spacing after any necessary grid stretching in the physical domain to allow more grid points within the boundary layer, if it exists, of a flow. Since $\mathbf{C}_0$ multiplies the highest powered eigenvalue k_x^3, it is found that the boundary points give a zero value on the main diagonal of $\mathbf{C}_0$ resulting in a singular matrix. To avoid the singular matrix and allow the technique to succeed, a transformation of the form

$$\lambda = (z_1 + k_x)/(z_2 - k_x)$$

is applied to equation (8) leading to the modified equation

$$\left[\mathbf{A}_0\lambda^3 + \mathbf{A}_1\lambda^2 + \mathbf{A}_2\lambda + \mathbf{A}_3\right]\mathbf{E} = 0 \tag{9}$$

where

$$\begin{aligned}
\mathbf{A}_0 &= \mathbf{C}_0 z_2^3 + \mathbf{C}_1 z_2^2 + \mathbf{C}_2 z_2 + \mathbf{C}_3 \\
\mathbf{A}_1 &= -3\mathbf{C}_0 z_1 z_2^2 + \mathbf{C}_1(z_2^2 - 2z_1 z_2) + \mathbf{C}_2(2z_2 - z_1) + 3\mathbf{C}_3 \\
\mathbf{A}_2 &= 3\mathbf{C}_0 z_1^2 z_2 + \mathbf{C}_1(z_1^2 - 2z_1 z_2) + \mathbf{C}_2(z_2 - 2z_1) + 3\mathbf{C}_3 \\
\mathbf{A}_3 &= -\mathbf{C}_0 z_1^3 + \mathbf{C}_1 z_1^2 - \mathbf{C}_2 z_1 + \mathbf{C}_3
\end{aligned}$$

In the transformation, z_2 cannot be equal to an eigenvalue k_x. Otherwise, we use the values $z_1 = z_2 = 1$. With this transformation, the $\mathbf{A}_0$ matrix is no longer singular. We can now left multiply equation (9) by $\mathbf{A}_0^{-1}$, define the vectors $\mathbf{E}_1 = \lambda\mathbf{E}$ and $\mathbf{E}_2 = \lambda\mathbf{E}_1$, and rearrange the system of equations to obtain

$$\left[\mathbf{A} - \lambda\mathbf{I}\right]\widetilde{\mathbf{E}} = 0 \tag{10}$$

where

$$\mathbf{A} = \begin{bmatrix} -\mathbf{A}_0^{-1}\mathbf{A}_1 & -\mathbf{A}_0^{-1}\mathbf{A}_2 & -\mathbf{A}_0^{-1}\mathbf{A}_3 \\ \mathbf{I} & \mathbf{0} & \mathbf{0} \\ \mathbf{0} & \mathbf{I} & \mathbf{0} \end{bmatrix}$$

is the companion matrix of order $3N + 3$ and

$$\widetilde{\mathbf{E}} = \begin{bmatrix} \mathbf{E}_2 & \mathbf{E}_1 & \mathbf{E} \end{bmatrix}^{\mathrm{T}}$$

is the eigen-vector for the companion matrix. The axial eigenvalues k_x and their associated eigen-functions are found from using the QR algorithm on the companion matrix $\mathbf{A}$ to obtain λ and applying the inverse transform. The eigen-functions $\mathbf{E}$ are obtained from the last third of the eigen-vector $\tilde{\mathbf{E}}$ and renormalized such that the L_2-norm of $\mathbf{E}$ equals 1. More specifically, the eigenvalues k_x are written as k_{xmn} where m is the circumferential mode number that is fixed for each solution of equation (6). The eigenvalues, for a fixed m, are ordered by the index n representing the radial mode order of the eigenvalue. Thus for a given mean flow profile, frequency, wall admittances, and circumferential mode number, we obtain all the axial eigenvalues and eigen-functions for each radial mode in the duct to some order of the discretization. The eigenvalues for higher modes become very inaccurate. The axial eigenvalues with the smaller magnitudes are of the most interest since they are associated with the lower order radial eigen-functions for which the Rotating Rake is designed to measure.

The eigenvalues produced by the companion matrix method are associated with all the modes that can propagate and/or decay in both directions in the duct. Since the current technique assumes that modes can propagate and decay only in one direction, the appropriate eigenvalues must be identified from the global set produced. Using the sign convention used for the exponential functions in equation (5), the following definitions are used to identify the appropriate eigenvalues. If k_x is complex, then the eigenvalues of physical interest are those that decay in the direction of propagation. These are identified by evaluating the imaginary part of k_x using the conditions

$$\begin{aligned} \Im\{k_x\} < 0 \qquad & \text{decay in } +x \text{ direction} \\ \Im\{k_x\} > 0 \qquad & \text{decay in } -x \text{ direction} \end{aligned} \tag{11}$$

If k_x is real, then the group velocity $c_g = \partial\omega/\partial k_x$ is computed to indicate the direction of propagation.

$$\begin{aligned} c_g > 0 \qquad & \text{propagation in } +x \text{ direction} \\ c_g < 0 \qquad & \text{propagation in } -x \text{ direction} \end{aligned} \tag{12}$$

Using c_g to determine the propagation direction takes into account the effect that a mean flow has on the propagation. A subset of lower-ordered eigenvalues representing modes propagating and/or decaying in the $+x$ direction is identified from the global set obtained and stored for use in the least-squares process.

Mode	Vo et al.[6]	$N = 200$
1	-1.5459i	-1.5459i
2	-5.2368i	-5.2368i
3	-8.4775i	-8.4775i
4	-11.6632i	-11.6632i
5	-14.8299i	-14.8299i
6	-17.9877i	-17.9877i
7	-21.1407i	-21.1407i
8	-24.2908i	-24.2907i
9	-27.4388i	-27.4387i
10	-30.5856i	-30.5853i

Hard wall, $m = 1$, $\eta = 1.0$, $M = 0.0$

Table 1. Comparison of k_x eigenvalues for modes propagating in the $+x$ direction.

Mode	Vo et al.[6]	$N = 200$
1	1.880 - 0.845i	1.8797 - 0.8450i
2	0.278 - 3.414i	0.2783 - 3.4141i
3	0.145 - 6.798i	0.1451 - 6.7979i
4	0.099 - 10.025i	0.0991 - 10.0248i
5	0.075 - 13.211i	0.0754 - 13.2106i
6	0.061 - 16.379i	0.0609 - 16.3793i
7	0.051 - 19.539i	0.0511 - 19.5392i
8	0.044 - 22.694i	0.0440 - 22.6940i
9	0.039 - 25.846i	0.0387 - 25.8456i
10	0.034 - 28.995i	0.0345 - 28.9949i

Soft wall, $\hat{A}_{ow} = 1.0 + 1.0i$, $m = 0$, $\eta = 1.0$, $M = 0.0$

Table 2. Comparison of k_x eigenvalues for modes propagating in the $+x$ direction.

II.B. Example Eigenvalue Problem Solutions

The computation of the eigenvalues and eigen-functions using the linear companion matrix method was performed with 5-point discretization at all interior and boundary points. This gives a fourth-order accurate solution. To validate the solution, test cases were run with increasing complexity. First, the eigenvalues were computed for a hard wall, cylindrical duct with no mean flow. The results are shown in Table (1) for

the $m = 1$ circumferential mode with $\eta = 1.0$, where $\eta = \omega R_o/c_r$ is a nondimensional frequency and c_r is a reference speed of sound. The comparison results are given from the fourth-order Runge-Kutta solution of Vo & Eversman.[6] The eigenvalues are identical to at least 3 decimal places. Next, the outer wall is made soft with a specific acoustic admittance $\hat{A}_{ow} = \rho_r c_r \hat{A}^*_{ow} = 1.0 + 1.0i$ where ρ_r is a reference density. The computed eigenvalues are identical to those from Vo & Eversman as shown in Table (2) for the $m = 0$ circumferential mode.

The problem complexity is increased by adding a constant mean flow to the soft wall circular duct. To represent the case of flow entering an inlet, the x-axis of the problem points out of the inlet while the flow enters in the opposite direction. Hence, the flow Mach number is set at a negative value, $M = -0.5$. The eigenvalues are shown in Table (3). The results are again identical to those from Vo & Eversman. (Note that the 10th mode from Vo & Eversman is actually the 14th mode. This was verified by observing the eigen-functions.)

+Mode	Vo et al.[6]	$N = 200$	-Mode	Vo et al.[6]	$N = 200$
1	0.620 - 5.014i	0.6195 - 5.0139i	1	0.410 + 1.290i	0.4101 + 1.2904i
2	-5.820 - 3.897i	-5.8195 - 3.8968i	2	1.259 + 6.085i	1.2595 + 6.0852i
3	0.445 - 9.187i	0.4453 - 9.1868i	3	1.146 + 9.668i	1.1457 + 9.6679i
4	0.453 - 13.062i	0.4539 - 13.0615i	4	1.022 + 13.315i	1.0218 + 13.3150i
5	0.480 - 16.822i	0.4795 - 16.8217i	5	0.943 + 16.977i	0.9425 + 16.9768i
6	0.503 - 20.531i	0.5029 - 20.5307i	6	0.891 + 20.635i	0.8907 + 20.6353i
7	0.522 - 24.213i	0.5220 - 24.2131i	7	0.855 + 24.288i	0.8549 + 24.2884i
8	0.538 - 27.880i	0.5376 - 27.8799i	8	0.829 + 27.937i	0.8288 + 27.9368i
9	0.550 - 31.537i	0.5503 - 31.5370i	9	0.809 + 31.581i	0.8089 + 31.5814i
10	0.589 - 49.754i	0.5608 - 35.1875i	10	0.755 + 49.772i	0.7933 + 35.2232i
14		0.5891 - 49.7539i	14		0.7546 + 49.7717i

Soft wall, $\hat{A}_{ow} = 0.72 + 0.42i$, $m = 2$, $\eta = 1.0$, $M = -0.5$

Table 3. Comparison of k_x eigenvalues. +Mode indicates mode propagating in the $+x$ direction against the flow. -Mode indicates mode propagating in the -x direction with the flow.

The possibility of including a shear flow in a duct is the advantage of the above numerical solution compared to the previous closed-formed, analytical solutions. This case was tested next. Previous eigenvalue results were available in Kousen[7] for a hard wall duct with a mean flow having a 1/7th power law profile.

$$M(r) = M(1 - r)^{(1/7)}$$

The computed eigenvalues are shown in Table (4) compared to the results from Kousen. The real eigenvalues and the imaginary parts of the complex eigenvalues are identical to 3 decimal places. The real parts of the complex eigenvalues are the same to 2 to 3 decimal places.

II.C. Least-Squares Fit

The microphone data from the Rotating Rake is Fourier analyzed to obtain complex values $p_m(r_i, \omega)$ that represent the separation of the acoustic pressure by frequency and circumferential mode order at each radial location, r_i, of the microphone. These values are expected to be functions of the radial mode content in the duct following

$$p_m(r_i, \omega) \approx \sum_{n=0}^{N_{max}-1} P_{mn}(\omega) E_{mn}(r_i; \hat{A}^*_{ow}, \hat{A}^*_{iw}, \omega), \qquad i = 1, 2, \ldots, N_{meas} \tag{13}$$

Equation (13) represents the attempt to further decompose the measured circumferential mode data into an approximate series of weighted radial basis functions computed using the linear companion matrix method as discussed above. These functions are not only functions of radial position and frequency, but are also functions of the outer duct wall admittance $\hat{A}^*_{ow}$ and, in the case of an annular duct, the inner duct wall

Mode	Kousen[7]	$N = 200$
1	0.81547	0.81527
2	0.76952	0.76948
3	0.72763	0.72758
4	0.65346	0.65339
5	0.54051	0.54043
6	0.36975	0.36966
7	0.06477	0.06481
8	-0.28277 + 0.48650i	-0.28309 + 0.48624i
9	-0.28328 + 0.80439i	-0.28366 + 0.80420i
10	-0.28368 + 1.0539i	-0.28415 + 1.05367i
11	-0.28403 + 1.2756i	-0.28459 + 1.27546i

Hard wall, $m = 0$, $\eta = 20.0$, $M = 0.3$

Table 4. Comparison of k_x/η eigenvalues for modes propagating in a duct containing a shear flow.

admittance $\hat{A}^*_{iw}$. To solve equation (13) for the complex radial mode amplitudes $P_{mn}(\omega)$, we use the least-squares method. For fixed admittances, the solution is to minimize the residual sum of squares

$$s = \|\mathbf{p} - \mathbf{BP}\|_2^2 \tag{14}$$

where

$$\mathbf{p} = \begin{bmatrix} \Re\{p_m(r_1)\} & \dots & \Re\{p_m(r_{N_{meas}})\} & \Im\{p_m(r_1)\} & \dots & \Im\{p_m(r_{N_{meas}})\} \end{bmatrix}^{\mathrm{T}}$$

is a real vector comprised of the real and imaginary parts of the measured complex circumferential mode data of length $n_p = 2N_{meas}$,

$$\mathbf{B} = \begin{bmatrix} \Re\{E_{m0}(r_1)\} & -\Im\{E_{m0}(r_1)\} & \dots & \Re\{E_{m(N_{max}-1)}(r_1)\} & -\Im\{E_{m(N_{max}-1)}(r_1)\} \\ \vdots & \vdots & \dots & \vdots & \vdots \\ \Re\{E_{m0}(r_{N_{meas}})\} & -\Im\{E_{m0}(r_{N_{meas}})\} & \dots & \Re\{E_{m(N_{max}-1)}(r_{N_{meas}})\} & -\Im\{E_{m(N_{max}-1)}(r_{N_{meas}})\} \\ \Im\{E_{m0}(r_1)\} & \Re\{E_{m0}(r_1)\} & \dots & \Im\{E_{m(N_{max}-1)}(r_1)\} & \Re\{E_{m(N_{max}-1)}(r_1)\} \\ \vdots & \vdots & \dots & \vdots & \vdots \\ \Im\{E_{m0}(r_{N_{meas}})\} & \Re\{E_{m0}(r_{N_{meas}})\} & \dots & \Im\{E_{m(N_{max}-1)}(r_{N_{meas}})\} & \Re\{E_{m(N_{max}-1)}(r_{N_{meas}})\} \end{bmatrix}$$

is a real matrix of coefficients derived from the radial basis functions of size $n_p \times n_c$, $n_c = 2N_{max}$, and

$$\mathbf{P} = \begin{bmatrix} \Re\{P_{m0}\} & \Im\{P_{m0}\} & \dots & \Re\{P_{m(N_{max}-1)}\} & \Im\{P_{m(N_{max}-1)}\} \end{bmatrix}^{\mathrm{T}}$$

is the real solution vector for the complex radial mode amplitudes of length n_c. By ensuring that the number of measurement points N_{meas} is greater than the number of radial basis functions N_{max}, the problem is overdetermined, $n_p > n_c$, and a solution to this linear problem is easily computed using the singular value decomposition method. This method provides the best approximation to solving the linear least-squares problem for over-determined systems and it is robust, handling problems where $\mathbf{B}$ is close to being singular. (See Lawson & Hanson[8] for details.)

II.D. Process for Nonlinear Least-Squares Fitting

In addition to the process of obtaining the complex modal amplitudes given the radial basis functions, it is desirable to deduce the wall admittance from the rotating rake measurements. There are cases where the wall admittance is not known or not known precisely where measurements could provide those values. At other times, a check of the installed wall admittance is required. To determine the wall admittance from

rotating rake data requires more extensive calculations than the linear least-squares fit to determine the mode amplitudes. The admittance (or its inverse, the impedance) appears in the boundary conditions of the governing equations. As such, the admittance affects the computed mode shapes, which are themselves, in essence, power series representations. Thus, the effect of varying the wall admittance appears nonlinearly in the mode solution. What was a linear least-squares solution to obtaining the mode amplitudes becomes a nonlinear, least-squares iterative solution. However, since only the admittances appear as nonlinear parameters, we can use conditional linearity to separate the fitting of the linear (the amplitude coefficients) and the nonlinear parameters.[9] This means that the iterative process required to solve a nonlinear least-squares problem is only applied to the nonlinear parameters.

Let f_i be the expectation function defined by the right hand side of equation (13). Using conditional linearity, we expand f_i into a Taylor's series about the current admittance values $\hat{\boldsymbol{\beta}}$ (a vector of length n_z) given the current amplitude values $\hat{\mathbf{P}}$

$$\mathbf{f}(\hat{\mathbf{P}}, \hat{\boldsymbol{\beta}} + \boldsymbol{\delta}) = \mathbf{f}(\hat{\mathbf{P}}, \hat{\boldsymbol{\beta}}) + \widetilde{\mathbf{B}}(\hat{\mathbf{P}}, \hat{\boldsymbol{\beta}})\boldsymbol{\delta} \tag{15}$$

where

$$\widetilde{B}_{ij} = \left.\frac{\partial f_i}{\partial \beta_j}\right|_{\hat{\mathbf{P}}, \hat{\boldsymbol{\beta}}} \quad i = 1, 2, \ldots, n_p \quad j = 1, 2, \ldots, n_z. \tag{16}$$

In these equations, $\mathbf{f}(\hat{\mathbf{P}}, \hat{\boldsymbol{\beta}})$ is determined from the linear least-squares solution outlined above for the current $\hat{\boldsymbol{\beta}}$ resulting in the current $\hat{\mathbf{P}}$, the best-fit amplitude coefficients for $\hat{\boldsymbol{\beta}}$. Thus, the amplitude coefficients are not held constant, but change to the best-fit values as $\boldsymbol{\beta}$ changes. Since equation (16) must be computed using numerical derivatives, additional calculations of $\mathbf{f}$ are required at incremental changes of each element of $\boldsymbol{\beta}$, all with the appropriate linear least-squares solution for $\mathbf{f}$. Once $\mathbf{f}$ and $\widetilde{\mathbf{B}}$ are computed, the system of equations is solved for the change $\boldsymbol{\delta}$ in the admittance values using least squares, computing the residual error at the new admittance values, and repeating until the error is minimized. While this iteration process is straight forward, in nonlinear least-squares problems it can be unstable and not converge to a minimum error solution. For instance, the computed $\boldsymbol{\delta}$ can be too large, sending $\mathbf{f}$ outside the local region of convergence. Thus, means are required to control the process.

Lawson & Hanson[8] detail using the method of Marquardt to solve this nonlinear least-squares problem and control the size of the steps that $\boldsymbol{\delta}$ can take. The equations are transformed and amended into the form

$$\begin{bmatrix} \mathbf{G}\widetilde{\mathbf{B}}\mathbf{D}^{-1} \\ \sqrt{\xi}\mathbf{I} \end{bmatrix} (\mathbf{D}\boldsymbol{\delta}) = \begin{bmatrix} \mathbf{G}\,(\mathbf{p} - \mathbf{f}) \\ \mathbf{0} \end{bmatrix} \tag{17}$$

where $\mathbf{G}$ is a diagonal matrix used for weighting the data. For example, it is common to give a relatively larger weight to terms in $(\mathbf{p} - \mathbf{f})$ that are considered more accurate. The diagonal matrix $\mathbf{D}$ is computed from the square root of the diagonal terms in $\widetilde{\mathbf{B}}^{\mathrm{T}}\mathbf{G}^{\mathrm{T}}\mathbf{G}\widetilde{\mathbf{B}}$. This matrix rescales the matrix $\widetilde{\mathbf{B}}$ to prevent erratic behavior in the convergence due to the possibility that $\widetilde{\mathbf{B}}$ may be nearly singular and causing large changes in $\boldsymbol{\delta}$. The ξ parameter moderates the step size taken by the impedance parameter $\boldsymbol{\beta}$ from the current parameters $\hat{\boldsymbol{\beta}}$ to the new parameters $\boldsymbol{\beta} = \hat{\boldsymbol{\beta}} + \boldsymbol{\delta}$.

Singular value decomposition is again used to solve for $\boldsymbol{\delta}$. Decompose the matrix $\mathbf{G}\widetilde{\mathbf{B}}\mathbf{D}^{-1}$ as

$$\mathbf{G}\widetilde{\mathbf{B}}\mathbf{D}^{-1} = \mathbf{U}\boldsymbol{\Sigma}\mathbf{V}^{\mathrm{T}}$$

where $\mathbf{U}$ contains the left singular vectors, $\mathbf{V}$ contains the right singular vectors, and $\boldsymbol{\Sigma}$ is a diagonal matrix containing the singular values σ_i. The step size vector $\boldsymbol{\delta}$ is then solved using the following three equations.

$$\begin{aligned} \hat{\mathbf{c}}_1 &= \mathbf{U}^{\mathrm{T}}\mathbf{G}\,(\mathbf{p} - \mathbf{f}) \\ y_i^{(\xi)} &= \sum_{j=1}^{n_z} V_{ij}\hat{c}_{1j}\frac{\sigma_j}{\sigma_j^2 + \xi} \quad i = 1, 2, \ldots, n_z \\ \delta_i &= \frac{y_i^{(\xi)}}{d_{ii}} \end{aligned}$$

As ξ is increased, the step size $\boldsymbol{\delta}$ is reduced to prevent divergence of the iteration. Alternatively, ξ can be reduced to promote faster convergence when possible. Thus, with appropriate choices for ξ as the iteration

progresses, systematic adjustments are made in both the nonlinear admittance parameters and the linear amplitude coefficients in order to reduce the error of the fit. Convergence to a solution is achieved when either

$$\left| \frac{s - \hat{s}}{\hat{s}} \right| < \epsilon,$$

the relative change in the residual sum of square errors, or

$$\left| \frac{\delta_i}{\beta_i} \right| < \epsilon \quad \text{for all } i,$$

the relative change in all the nonlinear parameters, is less than some chosen convergence tolerance ϵ.

This procedure for nonlinear least-squares fitting is based on the fact that the measured data is to be fit by a series of radial basis functions. As the conditions change in the duct, such as the mean flow and/or the wall admittance, the radial basis functions must be recomputed. Oftentimes, one can easily compute eigenvalues and eigen-functions by starting with a good initial guess eigenvalue and then tracking it through small changes in the duct conditions to the final desired condition. This could be easily accomplished by using the shooting or matrix method to solve the eigenvalue problem based on a reduced form of equation (6). The inverse power method would then be used to obtain the associated eigen-function. One could easily follow one or more modes using this approach with much less calculations then are performed here. However, such an approach often fails when the wall admittance is near 'optimum' where the theoretical maximum attenuation occurs for a particular frequency, geometry and input model content.[10]

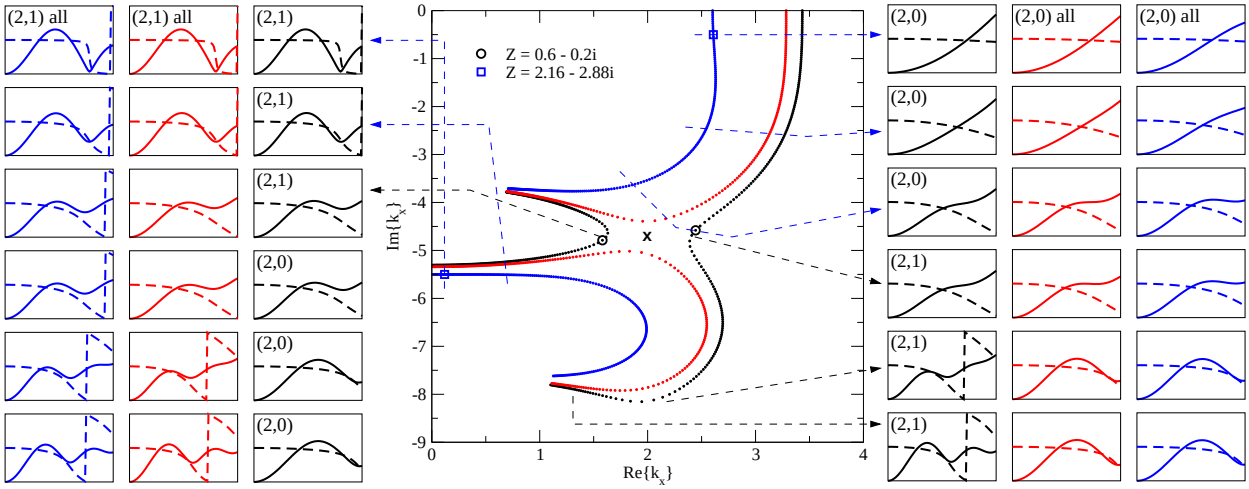

Figure 2. Trajectories of eigenvalues k_x for the 2 lowest radial modes as a function of the wall admittance $\hat{A}_{ow}$ where $\Im\{\hat{A}_{ow}\}$ is held constant. Black: $\Im\{\hat{A}_{ow}\} = 0.5$, Red: $\Im\{\hat{A}_{ow}\} = 0.45$, Blue: $\Im\{\hat{A}_{ow}\} = 0.22$; $m = 2$, $\eta = 3.6$, $M = 0.0$. The region where a double eigenvalue exists is marked with an 'X' bounded by $\Re\{\hat{A}_{ow}\} = 1.53$ and $\Im\{\hat{A}_{ow}\} = 0.45$ to 0.50. Side plots are radial basis functions at selected k_x values. Solid lines are magnitude. Dashed lines are phase.

The near-optimum admittance case is a test of the numerical methodology where conditions are changing rapidly. This is illustrated in Figure 2 where trajectories of the eigenvalue k_x are shown as a function of the wall admittance. In a manner following Zorumski & Mason,[11] the imaginary part of the admittance is held constant along the trajectory and every dot represents a 0.015 increment in the real part from the previous dot. Starting from $\Re\{\hat{A}_{ow}\} = 0$, the basis functions labeled $(2,0)$ have a real k_x, representing propagating duct modes. As $\Re\{\hat{A}_{ow}\}$ increases, the k_x trajectories leave the real axis with increasing amounts of damping. The basis functions labeled $(2,1)$ begin with an imaginary k_x, indicating that the duct modes are cut off. Their eigenvalues k_x move toward larger real parts as $\Re\{\hat{A}_{ow}\}$ increases. The condition for optimum admittance corresponds to the location of a double eigenvalue shown in the figure. As can be seen in this region, the eigenvalues change rapidly with small changes in admittance. Furthermore, the shapes of the basis function convert from one radial order to another as the trajectory passes near the double eigenvalue point.[12] In this example, the $(2,0)$ basis functions shown in black convert to $(2,1)$ basis functions as the black trajectory passes on the right side, larger $\Re\{k_x\}$ values, of the double eigenvalue. Conversely, on the left side, lower $\Re\{k_x\}$ values, the basis functions convert from a $(2,1)$ to a $(2,0)$ type of basis function. The consequence of this is that the eigenvalues and eigen-functions can change abruptly around near-optimum

admittance causing unstable conditions to occur in the nonlinear least-squares iteration. In the fitting process, it is the form of the radial basis functions that are fit to the data. It is the linear companion matrix method that produces these functions. Since we are not specifically concerned with what order the basis functions are listed, we can avoid the potential issue of 'mode-switching' by computing both the eigenvalues and the eigen-functions at each new admittance condition. The best fit of the basis functions to the data is then obtained by starting with one best fit basis function and then including additional best fit basis functions one at a time until the desired best fit overall is achieved. This process is illustrated in Figure 3 where data from measurements taken by the Rotating Rake in a hard wall duct are fit by computed radial basis functions. In Figure 3a, the first five radial basis functions are shown in the order computed by the linear companion matrix method. The third basis function has the lowest residual sum of square errors, $s = 197$, and is shown fit to the data on the right side with mode amplitude labeled $P_{4,0}$. Next, Figure 3b shows the remaining four basis functions. We now fit each of these functions to the data along with the part (a) function. The addition of the first basis function provides the smallest error, $s = 0.326$, and this mode amplitude is labeled $P_{4,1}$. The resulting total fit for the sum of the two modes is shown on the right side. Finally, part (c) shows the process repeated for the addition of a third basis function. For the fixed hard-wall boundary condition, this illustration is a repeated application of linear least-squares fitting of the computed basis functions as each additional basis function is included in the fit equation. In the nonlinear least-squares fitting, this process is performed at each iteration step as the wall impedance is varied to achieve best fit. While the mode amplitudes that gave minimum error were found directly, finding the best fit impedance through iteration requires a reasonable initial starting value.

III. Numerical Results

We next show two sets of numerical results for fitting computed radial basis functions to data. First, simulated data is used to test the fit process illustrated in Figure 3 for soft wall conditions. Second, data taken in the NASA Glenn Advanced Noise Control Fan (ANCF)[13] is used for fitting computed radial basis functions. The nonlinear least-squares fit process is used to find the best fit impedance for both constant, plug flow conditions and for mean flow profile conditions.

III.A. Simulated Data

The Eversman Inlet Radiation code[14] was used to generate mode propagation data along a treated section in a cylindrical duct. A (2,0) mode with a given amplitude was specified at the input plane of the duct. The duct initially had a hard wall followed by the treated section then reverting to a hard wall before the exit of the duct. The code computes the behavior of the initial mode as it propagates through the duct including scattering, reflection, and absorption. The magnitudes and phases of the pressures were extracted from the numerical data at the duct cross-section equal distance from the two ends of the treated section. Nine radial locations were selected to simulate microphone measurement points and the analysis was conducted for the $m = 2$ circumferential mode with $\eta = 3.6$ and $M = 0.0$. Two cases were computed: one non-optimum impedance, $Z = 2.16 - 2.88i$, and one near-optimum impedance, $Z = 0.6 - 0.2i$. Both wall impedance conditions used in the Eversman duct code calculations are indicated in Figure 2. Obviously, the non-optimum impedance is not near the double eigenvalue condition.

The duct code numerical data represents a simulation of the processed output from a rotating rake measurement, that is the complex pressures for one circumferential mode, the left side of equation (13). To illustrate the possibility of using the process for nonlinear least-squares iteration to determine a best fit wall impedance for the measured data, least-squares errors were computed as a function of the wall impedance. Figure 4 shows contour plots for the fit error using the non-optimum wall impedance data generated by the duct code. It is implicit in these results that the mode amplitudes, the $P_{mn}(\omega)$ factors in equation (13), are the best fit values for each wall impedance. At each impedance point used for computation on the grid, the process shown in Figure 3 is followed: first for one basis function, then two basis functions, and finally, three basis functions. All three cases show the same distinct minimum error region. Hence, these results show that the best fit wall impedance should be found in a straight forward manner using an iterative process where the error at each step is computed by a linear least-squares code using the most recent impedance. In this case, the best fit impedance would only change slightly whether 1, 2, or 3 radial basis functions were used in the fit.

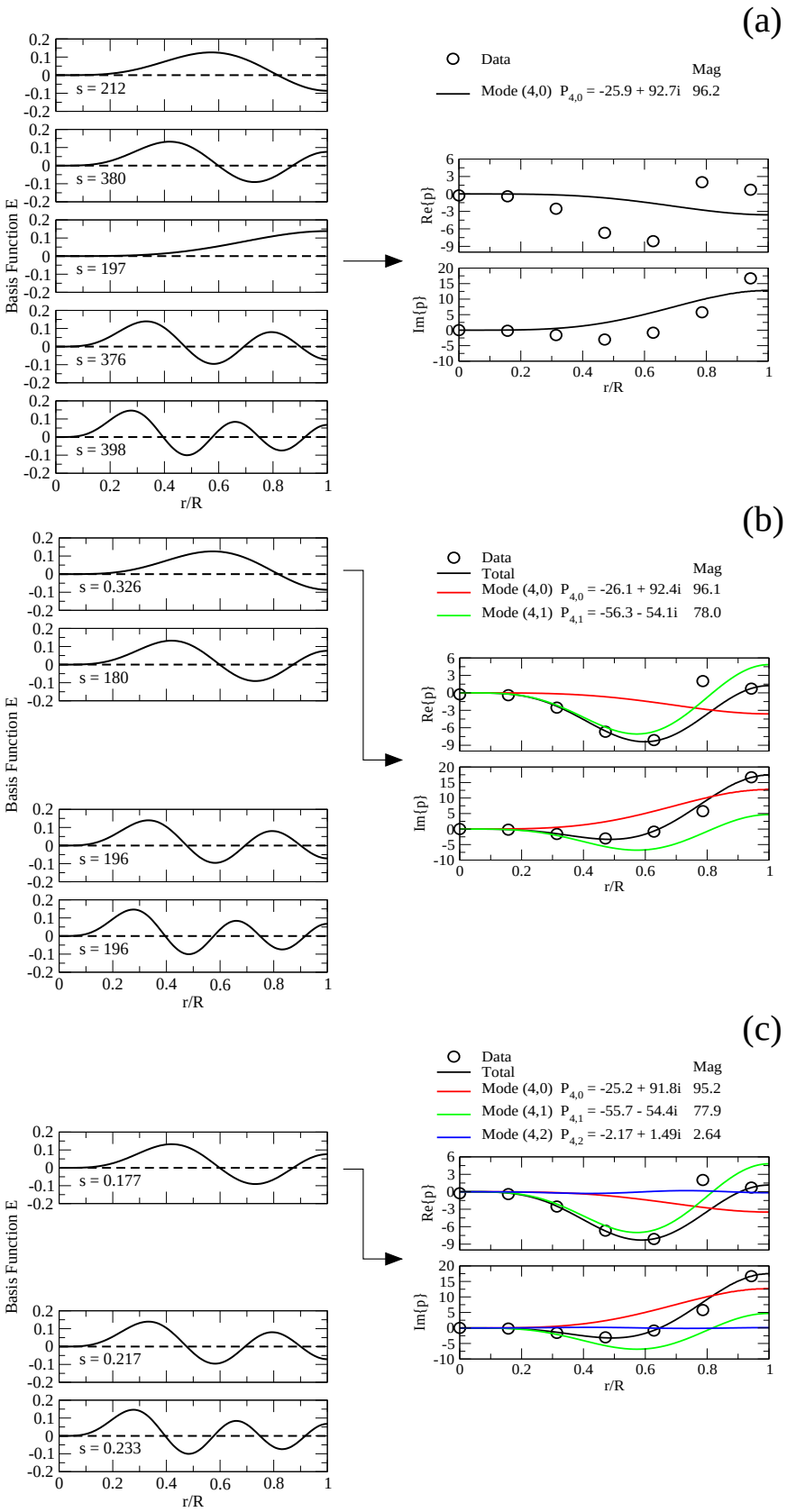

Figure 3. Process of fitting radial basis functions E_{mn} to data from Rotating Rake measurements in a hard wall duct. $m = 4$, $\eta = 10.8$, and $M = -0.115$. (a) Best fit one function. (b) Best fit second function given first function. (c) Best fit third function given first two functions. All basis functions are real. Mode amplitudes are complex.

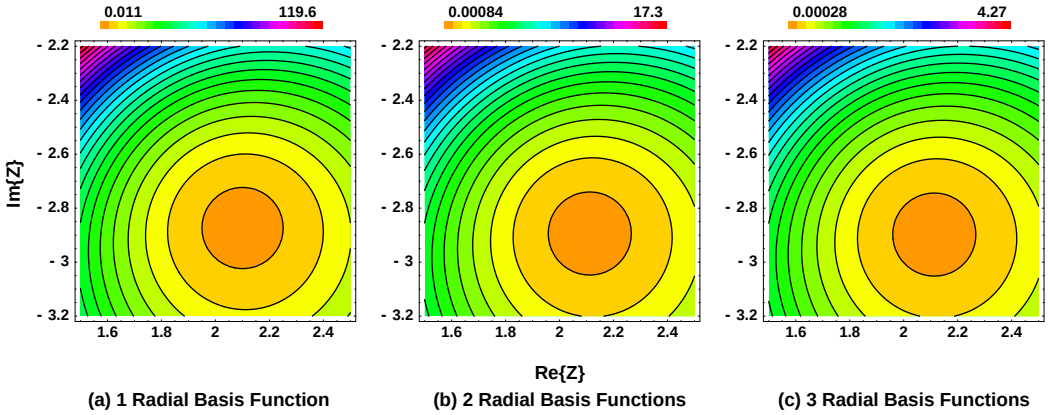

Figure 4. Contours of minimum least-squares fit error as a function of the wall impedance Z for 1, 2, or 3 radial basis functions (modes). Data was generated using input mode (2,0), wall impedance $Z = 2.16 - 2.88i$, $\eta = 3.6$, and $M = 0.0$.

Figure 5 shows the fit error contour plots using the duct code numerical data with the near-optimum wall impedance. In this case, more than one basis function is required to obtain a best fit wall impedance that has better agreement to the impedance used in the duct code. This result also illustrates that the fit process in the vicinity of the near-optimum impedance works well without regard to the 'mode-switching' behavior shown in Figure 2. The error contours are smooth indicating that the iterative process should not have problems progressing through to minimum error. Figure 5a may show the effects of 'mode-switching' as one basis function is fit in the impedance plane surrounding the double eigenvalue location, but this was not studied in detail at this time. For two or more basis functions, the effects of 'mode-switching' are not noticeable since the two basis functions are always present to balance each other to achieve the best fit. Thus, the results in Figures 5b and 5c behave more like the results in Figure 4 where adding more basis functions does not change the best fit impedance.

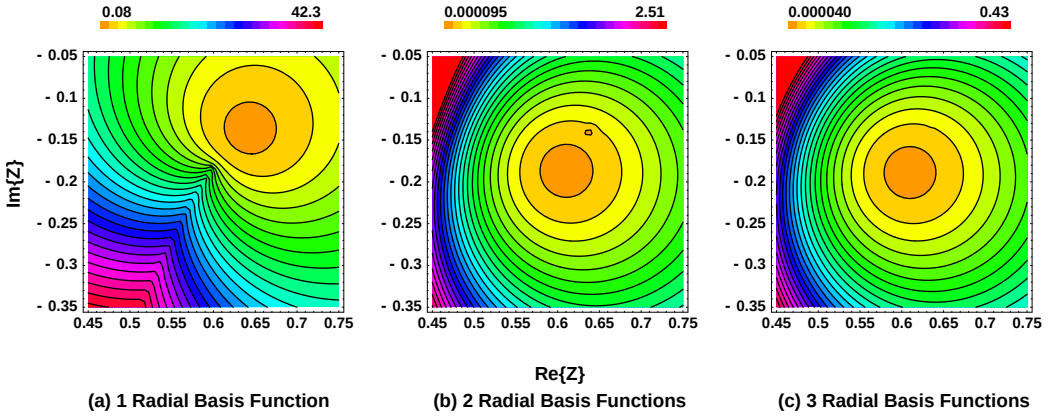

Figure 5. Contours of minimum least-squares fit error as a function of the wall impedance Z for 1, 2, or 3 radial basis functions (modes). Data was generated using input mode (2,0), wall impedance $Z = 0.6 - 0.2i$, $\eta = 3.6$, and $M = 0.0$.

III.B. Measured Data

The set of contour plots, shown in Figure 6, are computed fit errors resulting from using measured Rotating Rake data taken in the NASA Glenn Advanced Noise Control Fan (ANCF).[13] The wall treatment was a linear, single-degree-of-freedom liner with a screen mesh on a 34 percent open area perforate. For a fan speed of 1800 RPM, the duct plug flow Mach number was -0.115 and the design wall impedance was $Z = 1.7 - 2.4i$ for a normalized frequency of $\eta = 10.8$ corresponding to the second harmonic of the blade passage frequency. The $m = -8$ circumferential mode was used in this analysis. Unlike the previous results using computed simulated data, these results show significant changes in the error contour plots as the number of radial basis functions changes in the fit equation. For one basis function, the minimum error is in the vicinity of the

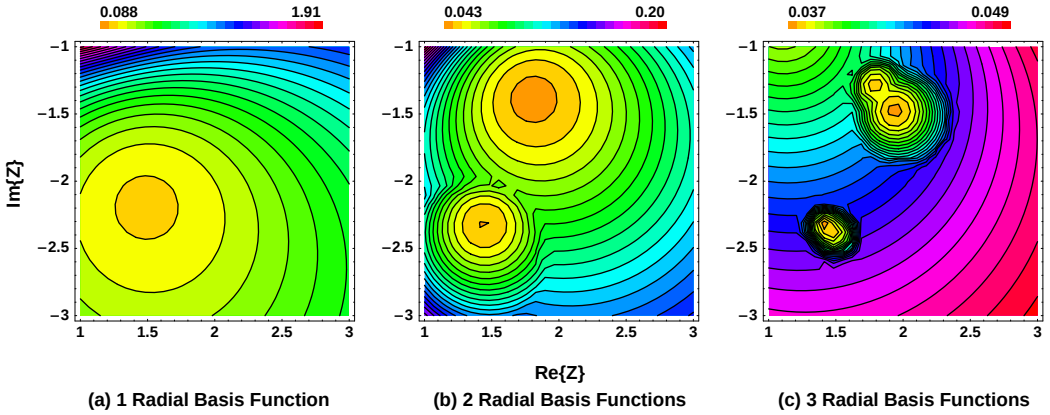

Figure 6. Contours of minimum least-squares fit error as a function of the wall impedance Z for 1, 2, or 3 radial basis functions (modes). Data from rotating rake measurements, $m = -8$, nominal wall impedance $Z = 1.7 - 2.4i$, $\eta = 10.8$, and $M = -0.115$.

nominal design impedance. Adding a second basis function to the fit gives rise to a second local minimum for best fit wall impedance within the search grid. With a third basis function, the two local minimum regions are smaller and distinct. While the color contours visually show the regions of minimum error, the range of actual error values is decreasing as more basis functions are added to the fit equation. Thus, given that each impedance point in Figure 6c has the best fit amplitudes for that impedance, then practically any point 'fits' the data even though there are two local minimum error regions since all the fit errors are reasonably small. To illustrate, the radial basis functions and the best fit modes amplitudes and shapes for these two conditions are shown in Figures 7a and 7b. In part (a), the $(-8, 0)$ mode fits the data very well by itself. (It should be noted that of the seven microphones the one microphone at $r/R = 0.943$ was determined after the testing to be not working properly. Hence, that data point was weighted such that it was set to zero.) Whereas in Figure 7b the addition of the $(-8, 1)$ mode is required to achieve a comparable level of fit. This results in a small 8 percent change, 0.7 dB, in the the dominant $(-8, 0)$ mode amplitude but the best fit impedance has changed about 36 percent. The small changes in mode amplitudes were enough to compensate for the changes in the radial basis functions due to the large change in the wall impedance to achieve a minimum fit error.

The same set of measured Rotating Rake data was analyzed again using a measured mean flow profile instead of plug flow. The flow profile is shown in Figure 9 with an average Mach number $M_{Avg} = -0.115$ (recalling that the flow is in the opposite direction of the positive x-axis.) The set of fit error contour plots are shown in Figure 8 and are contrasted to the equivalent set for plug flow conditions in Figure 6. Clearly for this condition the mean flow has affected the conditions for best fit wall impedance. Though it should be noted that the range of errors over the grid of impedances again becomes very small when two or more radial basis functions are used in the fit. Even though the contour plots can show dramatically different locations for best fit impedance, there is actually little change in the basic fit to the data. This is also illustrated in Figure 7. By adding only the effect of the mean flow profile at a constant wall impedance, we go from part (a) to part (c). The change in the shape of the basis functions is shown and the amplitudes of the modes have increased, a 2.5 dB increase for the $(-8, 0)$ mode, but the data is fit quite well. To achieve that last 10 percent reduction in error to get to the minimum error/best-fit-impedance condition required the real part of the impedance to increase 67 percent from 1.42 to 2.37. Thus, while the presence of the mean flow profile effects the shape of the radial basis functions, the limited amount of data included in the fit does not provide sufficient constraint allowing a large range of amplitude and impedance combinations to provide minimal fit errors. Other conditions were run to see if these kinds of changes occurred. The results for best fit impedance at three conditions are shown in Figure 10 compared to results from ANCF measured data analyzed using closed form basis functions and other measured and computed results previously presented in Sutliff.[13] Results are plotted at 747 Hz (at 1400 RPM, $M = -0.085$, $\eta = 8.4$, and $m = -4$), 853 Hz (at 1600 RPM, $M = -0.1$, $\eta = 9.6$, and $m = -8$), and 960 Hz (at 1800 RPM, $M = -0.115$, $\eta = 10.8$, and $m = -8$) for both the plug flow case and the flow profile case. For the two lower speed cases, the differences in the best fit impedance between the plug flow case and the flow profile case is much less than in the highest speed case. Also in both cases, the minimum error location was distinct as a function of the wall impedance. It is

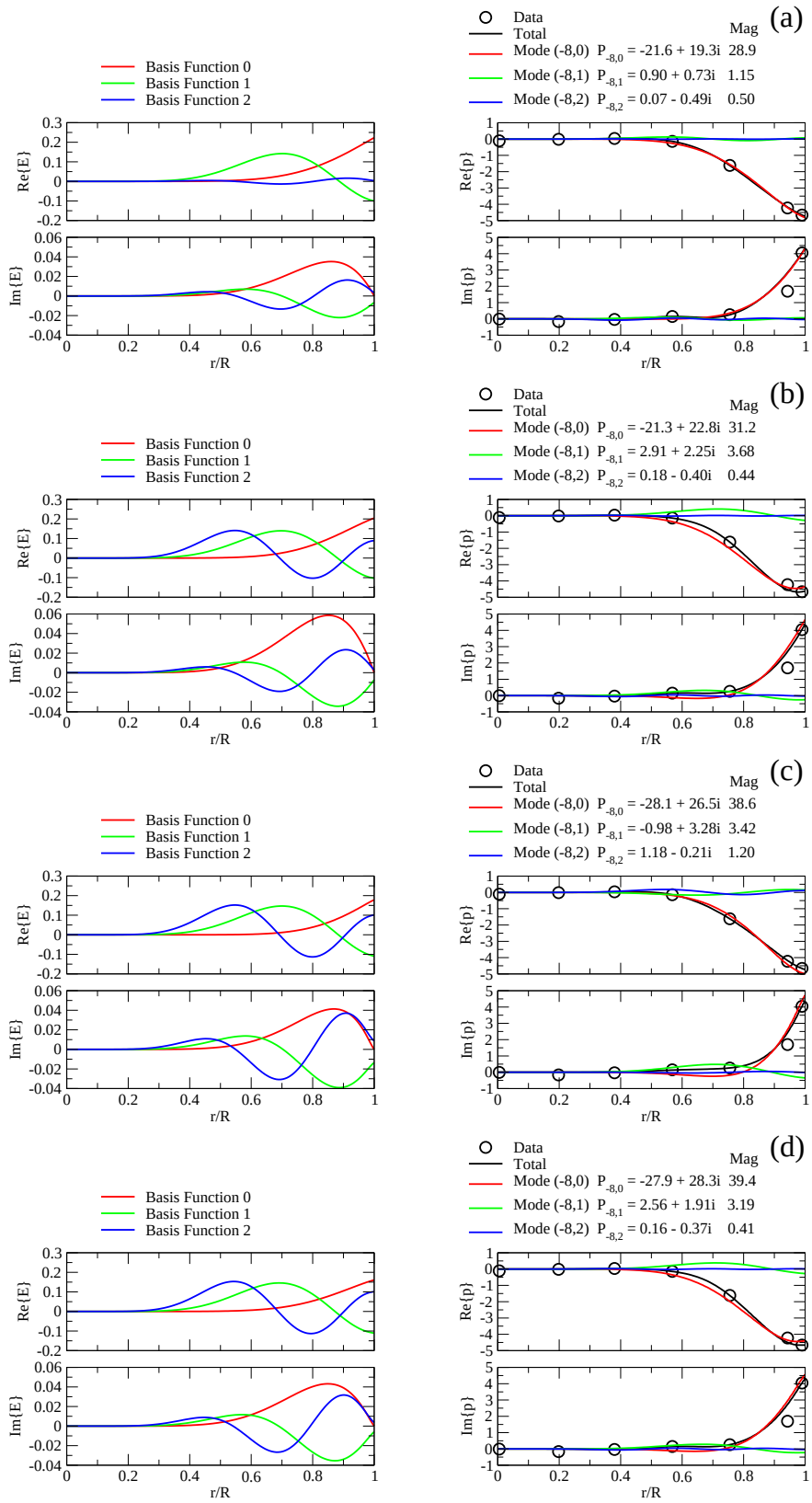

Figure 7. Changes in radial basis functions and mode fits with changes in wall impedance and flow conditions using data from Rotating Rake measurements in a soft wall duct. (a) Plug flow $M = -0.115$, best fit $Z = 1.42 - 2.32i$ near nominal wall impedance, $s = 0.0371$. (b) Plug flow $M = -0.115$, best fit $Z = 1.93 - 1.47i$, $s = 0.0372$. (c) Flow profile shown in Figure 9 with $M_{Avg} = -0.115$, wall impedance $Z = 1.42 - 2.32i$, $s = 0.0416$. (d) Flow profile shown in Figure 9 with $M_{Avg} = -0.115$, best fit $Z = 2.37 - 2.35i$, $s = 0.0373$.

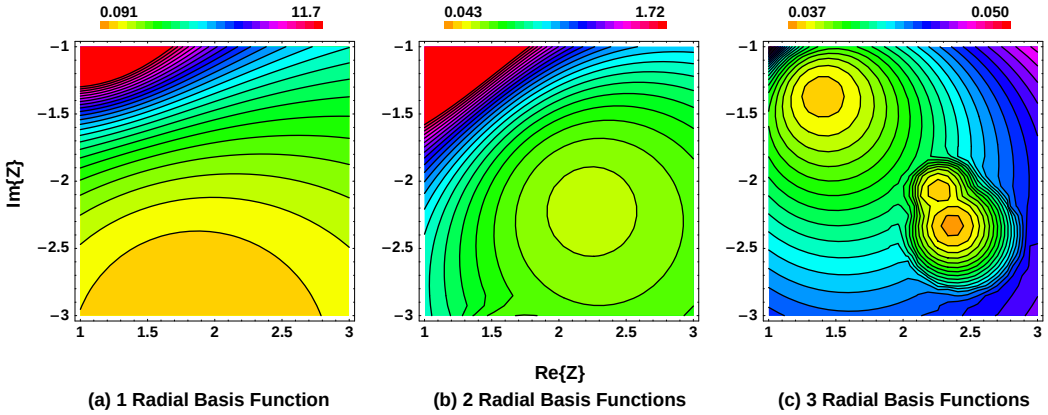

Figure 8. Contours of minimum least-squares fit error as a function of the wall impedance Z for 1, 2, or 3 radial basis functions (modes). Data from rotating rake measurements, $m = -8$, nominal wall impedance $Z = 1.7 - 2.4i$, $\eta = 10.8$, and $M_{Avg} = -0.115$ with mean flow profile shown in Figure 9.

not known if this is due to the lower flow speed or that the lower flow speed profiles are flatter as shown in Figure 9 for the $M_{Avg} = 0.085$ profile compared to the higher speed profile. More measurements at different frequencies and higher flow speeds are required. For these three in-duct, rotating rake measurements, the effect of the change in the flow profile, from plug flow to measured flow profile, and the effect of this flow on the boundary condition, equation (2), results in an increase in the measured wall resistance and an absolute increase in the measured wall reactance. Overall, the variability we see for the best fit impedances produced in this study is shown in Figure 10 to often be within the variability of the impedances measured by other techniques.

IV. Discussion

A numerical technique has been developed to compute the eigenvalues and eigen-functions for the duct solution with soft walls and a general mean flow. It uses the linear companion matrix method based on a discretization of the third-order governing equation and its boundary conditions. This method does not require an initial guess in order to solve the eigenvalue problem producing both the axial wave numbers, the eigenvalues, and their associated eigen-functions. The latter formed the basis functions that were used in the least-squares fit of the data. The results in this paper show that these basis functions can easily be used in a least-squares fit to determine the radial mode amplitudes as done in previous studies where closed form basis function solutions were used. With the numerically computed basis functions, the mean flow can be correctly accounted for whether it is a plug flow or a mean flow profile. It was shown in an example case using rotating rake measured data that when the mean flow profile is included, the mode amplitude increased 2.5 dB. This potential for changes in the mode amplitude has not yet been verified by measurements. It was mentioned above that once the mode amplitude is determined, the mode power can be calculated. Then assuming that the least attenuated modes are propagating out the duct, the in-duct mode power can be compared to far field radiated power. Thus, a check on the mode amplitude can be made with these measurements. This data could also provide a constraint on fitting the data to find the wall impedance.

While radiating mode power is useful, an issue of importance is that the results for best fit impedance assume that the modes are propagating in the direction out of the duct which is the same assumption used when duct radiating power is computed. When in-duct, rotating rake measurements are made over acoustic treatment, modes may exist in the local vicinity that are propagating in both directions due to reflections in the duct. Currently, these are all lumped together in the measured data. The analysis cannot separate modes propagating in opposite directions. It only computes mode amplitudes that best fits the basis functions given and it can have free reign to adjust the impedance as necessary to further improve the fit. This could be a reason why the fit error versus impedance grid search has such a low variability in the size of the error leading to the situation in Figure 7 where multiple fit solutions were found for the same data. A way to separate the direction of propagating modes is to take measurements at separate axial locations simultaneously.

Another issue to consider is that the expectation function for computing the residual sum of squares only used data from one circumferential m-order. Additional m-order equations can be included in equation

(14) each with their own circumferential mode data from rotating rake measurements and with their radial basis functions individually computed at the same frequency, wall admittance, and mean flow profile. With multiple radial basis functions competing to fit multiple sets of measured data all with the same impedance boundary condition (neglecting any effects of mode amplitude on the impedance), then perhaps the minimum error might be more definitive with errors away from minimum error being much larger than currently found in this study. Providing more data for the fit in that manner would be easier to do than, say, adding more microphones to the rotating rake. But, adding more microphones is still important for resolving higher orders of radial modes.

References

[1]Cicon, D. E., Sofrin, T. G., and Matthews, D. C., "Investigation of a Continuously Traversing Microphone System for Mode Measurement," NASA CR-168040, PWA-5846-26, November 1982.

[2]Sutliff, D. L., "Rotating Rake Turbofan Duct Mode Measurement System," NASA TM-2005-213828, October 2005.

[3]Hall, D. G., Heidelberg, L., and Konno, K., "Acoustic Mode Measurements in the Inlet of a Model Turbofan Using a Continuously Rotating Rake: Data Collection/Analysis Technique," AIAA Paper No. 93-0599, 1993.

[4]Eversman, W., "Theoretical Models for Duct Acoustic Propagation and Radiation," *Aeroacoustics of Flight Vehicles: Theory and Practice Volume 1: Noise Sources*, edited by H. H. Hubbard, NASA RP-1258, chap. 13, 1991.

[5]Bridges, T. J. and Morris, P. J., "Differential Eigenvalue Problems in Which the Parameter Appears Nonlinearly," *J. Comp. Physics*, Vol. 55, 1984, pp. 437–460.

[6]Vo, P. T. and Eversman, W., "A Method of Weighted Residuals with Trigonometric Basis Functions for Sound Transmission in Circular Ducts," *J. Sound Vib.*, Vol. 56, No. 2, 1978, pp. 243–250.

[7]Kousen, K. A., "Eigenmodes of Ducted Flows with Radially-Dependent Axial and Swirl Velocity Components," NASA CR-1999-208881, PWA-6420-108, March 1999.

[8]Lawson, C. L. and Hanson, R. J., *Solving Least Squares Problems*, Prentice-Hall, Englewood Cliffs, NJ, 1974.

[9]Bates, D. M. and Watts, D. G., *Nonlinear Regression Analysis and Its Applications*, Wiley, New York, NY, 1988.

[10]Rice, E. J., "Spinning Mode Sound Propagation in Ducts with Acoustic Treatment," NASA TN D-7913, 1975.

[11]Zorumski, W. E. and Mason, J. P., "Multiple Eigenvalues of Sound-Absorbing Circular and Annular Ducts," *J. Acoust. Soc. Am.*, Vol. 55, No. 6, 1974, pp. 1158–1165.

[12]Montétagaud, F. and Batard, H., "About the Complexity of Propagation and Radiation of Ducted Modes," AIAA Paper No. 2000-1955, 2000.

[13]Sutliff, D. L., "Rotating Rake Mode Measurements Over Passive Treatment in a Ducted Fan," NASA TM-2006-214493, December 2006.

[14]Topol, D. A. and Eversman, W., "TFaNS - Tone Fan Noise Design/Prediction System," NASA CR-1999-208883, PWA-6420-102, March 1999.

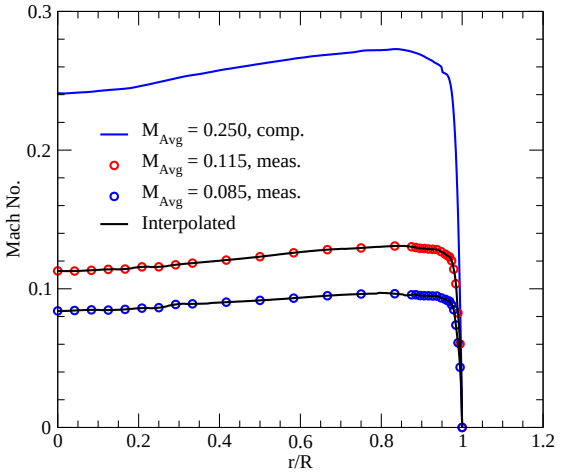

Figure 9. In-duct mean flow profiles. $M_{Avg} = 0.250$ **profile derived from CFD calculations.** $M_{Avg} = 0.115$ **and** 0.085 **profiles show measurement points in the ANCF with lines for interpolated results.**

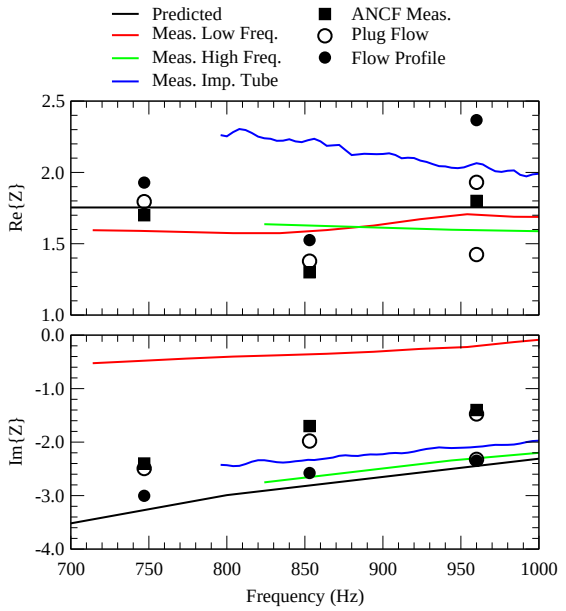

Figure 10. Wall impedance determined from best fit to Rotating Rake measured data. Open circle: plug flow calculations. Closed circle: flow profile calculations. All other data from Sutliff.[13]

REPORT DOCUMENTATION PAGE	Form Approved OMB No. 0704-0188

1. REPORT DATE *(DD-MM-YYYY)*	2. REPORT TYPE	3. DATES COVERED *(From - To)*
01-08-2007	Technical Memorandum	

4. TITLE AND SUBTITLE
Numerical Technique for Analyzing Rotating Rake Mode Measurements in a Duct With Passive Treatment and Shear Flow

5a. CONTRACT NUMBER

5b. GRANT NUMBER

5c. PROGRAM ELEMENT NUMBER

6. AUTHOR(S)
Sutliff, Daniel, L.; Dahl, Milo, D.

5d. PROJECT NUMBER

5e. TASK NUMBER

5f. WORK UNIT NUMBER
WBS 561581.02.08.03.03.01

7. PERFORMING ORGANIZATION NAME(S) AND ADDRESS(ES)
National Aeronautics and Space Administration
John H. Glenn Research Center at Lewis Field
Cleveland, Ohio 44135-3191

8. PERFORMING ORGANIZATION REPORT NUMBER
E-16130

9. SPONSORING/MONITORING AGENCY NAME(S) AND ADDRESS(ES)
National Aeronautics and Space Administration
Washington, DC 20546-0001

10. SPONSORING/MONITORS ACRONYM(S)
NASA; AIAA

11. SPONSORING/MONITORING REPORT NUMBER
NASA/TM-2007-214966; AIAA-2007-3679

12. DISTRIBUTION/AVAILABILITY STATEMENT
Unclassified-Unlimited
Subject Category: 71
Available electronically at http://gltrs.grc.nasa.gov
This publication is available from the NASA Center for AeroSpace Information, 301-621-0390

13. SUPPLEMENTARY NOTES

14. ABSTRACT
A technique is presented for the analysis of measured data obtained from a rotating microphone rake system. The system is designed to measure the interaction modes of ducted fans. A Fourier analysis of the data from the rotating system results in a set of circumferential mode levels at each radial location of a microphone inside the duct. Radial basis functions are then least-squares fit to this data to obtain the radial mode amplitudes. For ducts with soft walls and mean flow, the radial basis functions must be numerically computed. The linear companion matrix method is used to obtain both the eigenvalues of interest, without an initial guess, and the radial basis functions. The governing equations allow for the mean flow to have a boundary layer at the wall. In addition, a nonlinear least-squares method is used to adjust the wall impedance to best fit the data in an attempt to use the rotating system as an in-duct wall impedance measurement tool. Simulated and measured data are used to show the effects of wall impedance and mean flow on the computed results.

15. SUBJECT TERMS
Turbofan; Duct modes; Aeroacoustics; Measuring techniques; Acoustic impedance; Matrix methods

16. SECURITY CLASSIFICATION OF:			17. LIMITATION OF ABSTRACT	18. NUMBER OF PAGES	19a. NAME OF RESPONSIBLE PERSON
a. REPORT	b. ABSTRACT	c. THIS PAGE			STI Help Desk (email:help@sti.nasa.gov)
U	U	U	UU	22	19b. TELEPHONE NUMBER *(include area code)* 301-621-0390